Contrasting Characteristics of the Surface Energy Balance between the Urban and Rural Areas of Beijing

WANG Linlin[1,2], GAO Zhiqiu*[1], MIAO Shiguang[3], GUO Xiaofeng[1], SUN Ting[4], Maofeng LIU[5], and Dan LI[6]

[1]*State Key Laboratory of Atmospheric Boundary Layer Physics and Atmospheric Chemistry, Institute of Atmospheric Physics, Chinese Academy of Sciences, Beijing* 100029

[2]*Collaborative Innovation Center on Forecast and Evaluation of Meteorological Disasters, Nanjing University of Information Science & Technology, Nanjing, Jiangsu* 210044

[3]*Institute of Urban Meteorology, China Meteorological Administration, Beijing* 100089

[4]*State Key Laboratory of Hydroscience and Engineering, Department of Hydraulic Engineering, Tsinghua University, Beijing* 100084

[5]*Department of Civil and Environmental Engineering, Princeton University, Princeton, NJ* 08540*, USA*

[6]*Program of Atmospheric and Oceanic Sciences, Princeton University, Princeton, NJ* 08540*, USA*

(Received 28 March 2014; revised 15 August 2014; accepted 19 August 2014)

ABSTRACT

A direct comparison of urban and rural surface energy balances, as well as a variety of other variables including incoming shortwave/longwave radiation and aerosol optical depth, is conducted for the Beijing metropolitan area. The results indicate that, overall, the urban area receives a smaller amount of incoming shortwave radiation but a larger amount of incoming longwave radiation. However, comparisons in the aerosol optical depth and cloud fraction at the two locations suggest that neither aerosol optical depth nor cloud fraction alone can explain the difference in the incoming shortwave radiation. The urban–rural differences in the incoming longwave radiation are unlikely to be caused by the presence of more abundant greenhouse gases over the urban area, as suggested by some previous studies, given that water vapor is the most dominant greenhouse gas and precipitable water is found to be less in urban areas. The higher incoming longwave radiation observed over the urban area is mostly likely due to the higher temperatures of the ambient air. The urban area is also found to always produce higher sensible heat fluxes and lower latent heat fluxes in the growing season. Furthermore, the urban area is associated with a larger amount of available energy (the sum of sensible and latent heat fluxes) than the rural area, except in May and October when evapotranspiration in the rural area significantly exceeds that in the urban area. This study provides observational evidence of urban–rural contrasts in relevant energy-balance components that plausibly arise from urban–rural differences in atmospheric and land-surface conditions.

Key words: aerosol load, cloud, evapotranspiration, surface energy balance, urbanization

Citation: Wang, L. L., Z. Q. Gao, S. G. Miao, X. F. Guo, T. Sun, M. F. Liu, and D. Li, 2015: Contrasting characteristics of the surface energy balance between the urban and rural areas of Beijing. *Adv. Atmos. Sci.*, **32**(4), 505–514, doi: 10.1007/s00376-014-3222-4.

1. Introduction

The past few decades have seen increasing interest in urban meteorology and hydrology (Arnfield, 2003; Britter and Hanna, 2003; Shephard, 2005; Grimmond, 2007; Kanda, 2007; Zhang et al., 2011); part of the motivation stems from the fact that the ever-growing urban population and global climate change have posed significant challenges to sustainable energy and water resources in metropolitan areas worldwide (Grimm et al., 2008). Understanding the interactions between the complex, heterogeneous urban surface and the overlying atmosphere is essential for addressing many urban environmental issues (Li and Bou-Zeid, 2013; Li et al., 2013), and is also critical for improving numerical weather and climate models as well as air quality models (Miao et al., 2009; Grimmond et al., 2010; Chen et al., 2011; Grimmond et al., 2011).

A direct comparison between urban and rural surface energy balances [Eq. (1)] is especially important for understanding the peculiar features of urban surfaces and the impact of urbanization (Oke, 1982). The one-dimensional surface energy balance is usually formulated as

$$Q = H + \mathrm{LE} + G\,, \tag{1}$$

where Q is the driving energy flux, H is the sensible heat flux from the surface to the adjacent air, LE is the latent heat flux

* Corresponding author: GAO Zhiqiu
Email: zgao@mail.iap.ac.cn

into the atmosphere associated with evapotranspiration, and G is the ground and urban canopy heat storage. $Q = R_n + Q_F$, where R_n is the net radiation resulting from the imbalance between the incoming and outgoing radiation [see Eq. (2)] and Q_F is the anthropogenic heat flux that is often non-negligible in urban settings. Q_F can be obtained by an energy consumption survey, based on building energy model and transportation system model calculations. R_n is expressed as

$$R_n = SW_{in} + LW_{in} - SW_{out} - LW_{out} , \quad (2)$$

where SW_{in} is the downwelling shortwave radiation, LW_{in} is the downwelling longwave radiation, SW_{out} is the upwelling shortwave radiation, and LW_{out} is the upwelling longwave radiation. The framework proposed by Oke (1982) remains the paradigm for understanding the difference between urban and rural surface energy balances. Compared to peri-urban and rural areas, the incoming shortwave and longwave radiation fluxes are notably influenced in urban areas due to, in particular, the presence of atmospheric pollutants. Meanwhile, the outgoing shortwave and longwave radiation fluxes are modified primarily by changes in surface radiative properties. The partitioning of the driving energy flux into the sensible heat flux, latent heat flux and ground heat flux is shifted in favor of the sensible heat flux and the ground heat flux. Furthermore, the latent heat flux is significantly reduced in urban areas due to the extensive use of impervious materials such as asphalt and concrete. The boundary-layer stability also plays a role in causing differences in the sensible heat flux between urban and rural areas, especially during nighttime (Hu et al., 2013).

In practice, the urban surface energy balance is also closely dependent on the urban morphology and has been found to vary from place to place [see Piringer et al. (2002) for a review]. It also varies seasonally due to the variability of surface properties (such as vegetation coverage) as well as climate conditions (Loridan and Grimmond, 2012; Miao et al., 2012). Therefore, the urban–rural contrast cannot be expected to be universal across different geographic locations and may also vary seasonally and even over longer time scales. Numerous studies have investigated into characteristics of the urban surface energy balance and documented a diversity of differences from the rural counterparts [see Oke (1982) and Piringer et al. (2002) for reviews]. Nonetheless, most previous studies are devoted to developed countries and cover relatively short time periods (Cleugh and Oke, 1986; Grimmond et al., 1993; Grimmond and Oke, 1995; Grimmond and Oke, 1999; Loridan and Grimmond, 2012; Nordbo et al., 2013). Recently, several field experiments were conducted in densely populated megacities for extended periods of time (e.g., Kanda et al., 2002; Wood et al., 2010; Miao et al., 2012). Some of these experiments have multiple observational sites located over different land-cover types within urban environments and span a number of years. In this study, we try to address differences in the urban and rural surface energy balances over the Beijing metropolitan area using observation data available over the entire year of 2011.

Over the past few decades, Beijing, the capital of China, has been amongst the fastest growing cities in the world. In 2010, the number of permanent residents of Beijing exceeded 19.6 million and the population density in downtown Beijing reached 23 400 km^{-2}, according to the results of the sixth national census of China (OSCB, 2011). The rapid urbanization of Beijing has caused numerous environmental problems such as air pollution and soil degradation, which might also play a role in affecting the surface energy balance (Tan and Li, 2013). In addition, many studies have documented potential impacts of the urbanization on aerosol load, boundary-layer stability, cloud formation, and rainfall climatology (Shephard, 2005; Rosenfeld et al., 2008; Zhang et al., 2009; Miao et al., 2011; Hu et al., 2013), which are closely associated with changes in the surface energy balance. Therefore, characterizing the urban surface energy balance and comparing it to its rural counterpart is important and can shed light on many environmental problems in the Beijing metropolitan area.

The objective of this study is to examine differences in the urban and rural surface energy balances over the Beijing metropolitan area. To provide a comprehensive comparison, the urban–rural contrasts in terms of the aerosol load and cloud conditions are also examined in view of their strong influences on the surface energy balance. This paper is organized as follows: Section 2 describes the observational datasets and methodology, followed by presentation and interpretation of the main results in section 3. The discussion and conclusions are given in section 4.

2. Data and methodology

2.1. *Site description*

The data used in this study are available from field measurements at an urban site (39.97°N, 116.37°E, the Beijing "inner-city" site) and a rural site (39.75°N, 116.96°E, the Xianghe "peri-urban" site) over the Beijing metropolitan area, China. The two sites are about 60 km apart. The Beijing flux tower is 325 m high, and is officially known as "the Beijing 325-m meteorological tower". It conducts turbulent flux measurements at three different levels: 47 m, 140 m and 280 m above ground level. The Xianghe tower is 102 m high, and conducts turbulence measurements at two different levels: 32 m and 64 m. The geographic locations of these two towers and adjacent land-cover features are shown in Fig. 1. The land-use and land-cover information is available from the FROM-GLC (Finer Resolution Observation and Monitoring of Global Land Cover) dataset, which is the first 30 m resolution global land-cover product derived from Lands at Thematic Mapper (TM) and Enhanced Thematic Mapper Plus (ETM+) observations (Gong et al., 2012). It is worthwhile to characterize the land-cover information within the footprints of the measurements. The spatial representativeness of observed fluxes or concentrations above the surface can be quantified using the footprint function. The upwind fetch needed by flux measurements at different heights can be evaluated based on the growth of the internal boundary and equilibrium layers, whose vertical ranges grow roughly

as 1/10 x and 1/100 x, respectively [x is the upwind fetch length; see Brutsaert (1982)]. As a result, we estimate the footprint as a rectangle with an area of 100 z × 100 z that is centered on the flux tower (the distance from the flux tower to each edge is 50 z, where z is the measurement height). Given that no simple model exists for estimating footprints over heterogeneous surfaces, such an empirical approach for estimating the footprint is deemed sufficient in our study. The two footprints shown in Fig. 1 correspond to measurements made at 280 m and 64 m, which provide top-level turbulent flux measurements at the Beijing and Xianghe sites, respectively. The land-use fractions within the footprints of each measurement height at the two sites are provided in Table 1. It is clear that fractions of impervious surface at the Beijing site range from 65% to 82% in the three footprints (47 m, 140 m and 280 m) and decrease with an increase in height. Vegetated surfaces at the two sites are comprised mainly of cropland/grassland. For the Beijing site, the vegetated surface fractions range from 12% to 29% and increase with an increase in height. For the Xianghe site, croplands constitute the highest fractions and have no significant differences between the two footprints (32 m and 64 m). Compared to the Beijing site, surface compositions for the different footprints at the Xianghe site are much more homogeneous.

Wang et al. (2014) analyzed the surface composition of the footprints of the Beijing flux tower using 30 m resolution Landsat TM5 satellite images. In their analysis, three land-cover types are distinguished: impervious surface, soil, and vegetated surface. The fractions of impervious surfaces range from 65% to 75% in the three footprints for the three levels. Soil is the second most important surface type, with fractions ranging from 20% to 30%. Vegetated surfaces represent the lowest fraction (about 5%). Our estimates herein are in broad agreement with Wang et al. (2014), given that soil and vegetated surfaces are not distinguished in this study.

As shown in Table 1, the Xianghe site is surrounded primarily by cropland (about 75%), while the impervious surface fraction is small (about 20%) and is primarily located to the east of the tower. The surface compositions of the two footprints for the two levels at the Xianghe site are very similar.

Table 1. Land-use fractions within the footprints of each flux measurement height at the two sites.

	z (m)	Cropland (%)	Impervious (%)	Water (%)	Others (%)
Beijing	47	12	82	6	0
	140	18	74	7	1
	280	29	65	4	2
Xianghe	32	75	22	1	2
	64	74	21	3	2

2.2. *Observational datasets*

2.2.1. *Turbulent fluxes*

The field measurements and related experimental details at the Beijing flux tower have been reported elsewhere (Li et al., 2010; Miao et al., 2012). High-frequency measurements of wind velocity, air temperature, water vapor and CO_2 concentrations are available through combinations of three-dimensional sonic anemometers (Campbell Scientific CSAT3, USA) and open-path gas analyzers (LICOR-7500, USA). Similarly, at the Xianghe site, wind velocity and air temperature are measured using three-dimensional sonic anemometers (Gill, UK), while water vapor and CO_2 concentrations are measured using open-path gas analyzers (LICOR-7500, USA).

Turbulence data are recorded at a frequency of 10 Hz. Double rotation (i.e., yaw and pitch rotations) and linear detrending are applied to all time series. Webb correction is applied to the water vapor and CO_2 fluxes. The processing of turbulence data follows the method described in Wang et al. (2014).

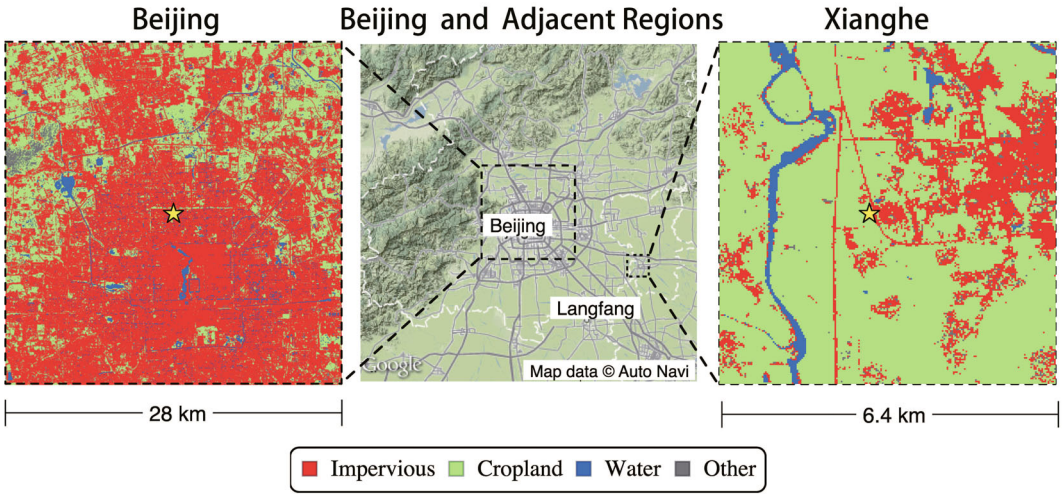

Fig. 1. The land cover at the Beijing and Xianghe sites given by the FROM-GLC. The two stars are the locations of the towers. The middle panel shows the geographic features of the Beijing and Adjacent Regions (courtesy of Google).

2.2.2. *Radiation*

At the Beijing site, four-component radiation (i.e., incoming shortwave and longwave radiation, and outgoing shortwave and longwave radiation) is also measured at the three levels using CNR1 radiometers. At the Xianghe site, the radiation measurements only include incoming shortwave and longwave radiation. The incoming shortwave radiation is derived by summing the direct and diffuse components, which are measured using an Eppley Normal Incidence Pyrheliometer and a black-and-white radiometer. The incoming longwave radiation is measured using an Eppley Precision Infrared Radiometer. Additional information about the instruments and data quality control can be found in Xia et al. (2007). Note that the global incoming shortwave radiation measured by the Kipp–Zonen CM21 and CM11 radiometers at the Xianghe site are not used in this study, as recommended in Xia et al. (2007).

2.2.3. *Aerosol optical depth and precipitable water*

Both sites are part of the Aerosol Robotic Network (AERONET, http://aeronet.gsfc.nasa.gov/) and have cloud-screened observations of aerosol optical depth (AOD) and precipitable water (Holben et al., 1998; Eck et al., 1999; O'Neill et al., 2003). AOD is a measure of radiation extinction through an air column. It is an indicator for aerosol load in the atmosphere: the higher the AOD values, the more aerosols are present in the atmosphere. AODs at different wavelengths (340, 380, 440, 500, 675, 870 and 1020 nm) are retrieved in the AERONET products and the uncertainty associated with AOD observations is about 0.01–0.02 (Eck et al., 1999). For this study, only AODs at 440, 675, 870 and 1020 nm from the Level 2.0 product are used, due to data availability. The precipitable water is the integrated water vapor amount in the air column and is derived from the 935 nm channel at AERONET sites.

2.2.4. *Cloud observations*

Cloud information at the two sites is provided by Moderate Resolution Imaging Spectroradiometer (MODIS) satellite observations. In this study, we are particularly interested in the urban–rural contrasts in cloud coverage. As such, the instantaneous global Level 2 product MOD06_L2 is used (http://modis-atmos.gsfc.nasa.gov/MOD06_L2/index.html), which estimates the 5 min cloud fraction at a 5 km resolution from a CO_2 slicing technique for both daytime and nighttime. The cloud fraction is provided at a frequency of two to four times every day.

2.3. *Turbulent flux calculation*

The friction velocity u_* is calculated using $u_* = (\overline{u'w'}^2 + \overline{v'w'}^2)^{1/4}$. The sensible heat, latent heat and carbon dioxide fluxes are calculated using the eddy-covariance method:

$$H = \rho c_p \overline{w'T'}\,, \tag{3}$$

$$\mathrm{LE} = \rho L_v \overline{w'q'}\,, \tag{4}$$

$$\mathrm{CFX} = \overline{w'c'}\,, \tag{5}$$

where u, v, and w are the streamwise, cross-stream and vertical velocities (m s^{-1}), respectively; T is the temperature (K); q is the specific humidity (kg kg^{-1}); and c is the concentration of CO_2 (mg m^{-3}). The overbar denotes time averages and an averaging period of 30 minutes is used in this study. The prime denotes turbulent fluctuations from the Reynolds averages. ρ is the air density (kg m^{-3}). c_p is the specific heat capacity at constant pressure (J kg^{-1} K^{-1}) and L_v is the latent heat for moisture exchange (J kg^{-1}).

Following Li and Bou-Zeid (2011) and Wang et al. (2014), only the data satisfying the following criteria are used: $|u_*| > 0.1$ m s^{-1}, $|H| > 10$ W m^{-2}, $|\mathrm{LE}| > 10$ W m^{-2} and $|\mathrm{CFX}| > 0.01$ mg m^{-2} s^{-1}. Unusually large turbulent fluxes are also excluded from the analyses, since they are likely to be associated with measurement problems. In our study, sensible and latent heat fluxes greater than 400 W m^{-2} or less than -200 W m^{-2} are excluded. Given that we do not have information about the anthropogenic heat flux, the heat storage G in Eq. (1) is simply calculated as $R_n - H - \mathrm{LE}$.

3. Results

3.1. *Radiative energy components at the urban and rural sites*

We first examine the incoming shortwave and longwave radiation at the two sites. Figure 2 compares the monthly-averaged diurnal cycles of the incoming shortwave and longwave radiation at the urban and rural sites. As seen in Fig. 2, diurnal variations of the incoming shortwave and longwave radiation at the two sites are fairly similar. Nonetheless, their magnitudes are evidently different between the two sites. As presented in Fig. 3, which shows the monthly-averaged differences between the two sites in terms of incoming shortwave and longwave radiation, the urban site receives less shortwave radiation but more longwave radiation than the rural site. The incoming shortwave radiation at

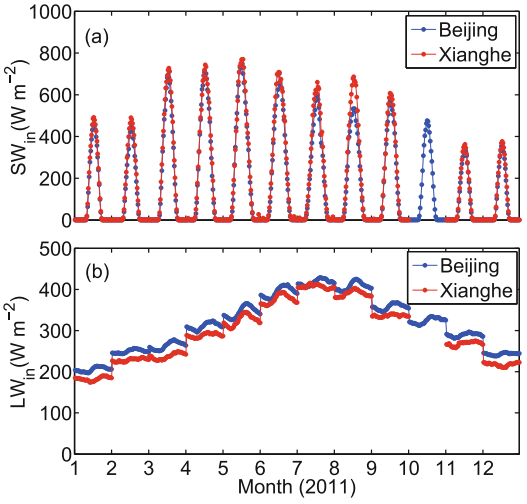

Fig. 2. Monthly-averaged diurnal cycles of incoming shortwave and longwave radiation at the Beijing and Xianghe sites in 2011.

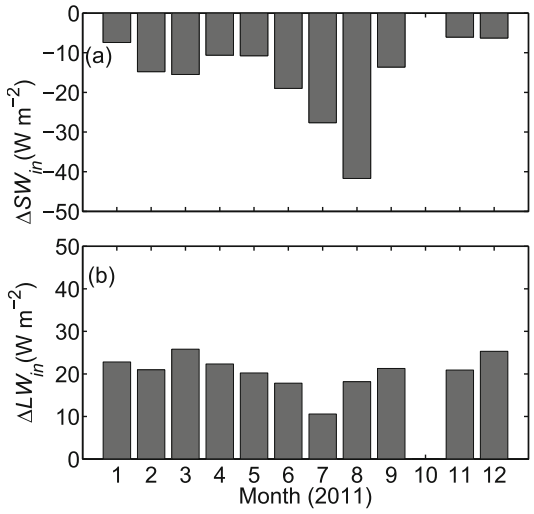

Fig. 3. Monthly-averaged differences in incoming shortwave and longwave radiation at the Beijing and Xianghe sites in 2011.

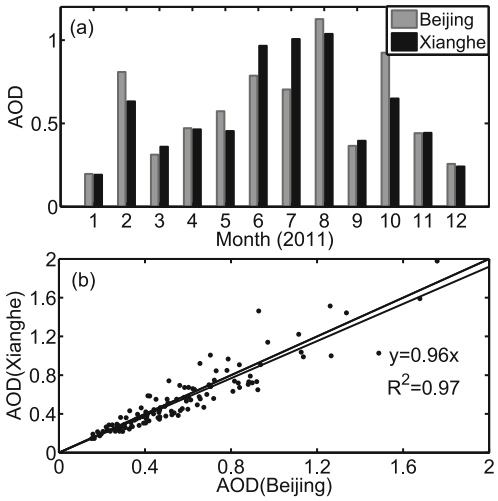

Fig. 4. (a) Monthly-averaged AOD at the Beijing and Xianghe sites at 675-nm wavelength in 2011, and (b) comparison of monthly-averaged AOD at Beijing and Xianghe at four wavelengths (units: nm) from 2010 to 2012.

the urban site is about 20% lower in August and about 3% to 12% lower in other months during the daytime (0800–1700 LST). The incoming longwave radiation at the urban site is about 3% to 15% larger than that at the rural site during the daytime (0800–1700 LST). The maximum (15%) occurs in January and the minimum (3%) in July. According to Oke (1982), the incoming shortwave radiation is typically 2% to 10% lower in the city (Peterson and Stoffel, 1980), while the incoming longwave radiation is slightly increased as a result of urbanization. Our results are in agreement with the descriptions by Oke (1982). It is interesting to observe that the differences between the urban and rural incoming shortwave radiation exhibit some seasonal variability, as can be seen from Fig. 3. The differences are larger in boreal summer than in winter, and are most evident in August. Nonetheless, the differences in incoming longwave radiation show less seasonal variability, with those in winter only slightly larger than those in summer.

To assess the impact of urbanization on the atmospheric conditions, we investigate the aerosol, precipitable water and cloud measurements at the two sites. These variables can potentially have significant impacts on the surface energy balance. For example, a higher level of AOD and cloud fraction will result in lower incoming shortwave radiation at the surface; while a higher level of precipitable water will increase the incoming longwave radiation at the surface. The monthly-averaged AODs measured at four different wavelengths (1020 nm, 870 nm, 675 nm and 440 nm) at the two sites in 2011 were compared and the results are similar for these four wavelengths. Hence, only AODs at 675 nm are shown in Fig. 4a. As can be seen from Fig. 4a, the AOD values are generally larger in summer than in other seasons, which is consistent with the observations in Che et al. (2009). In summer, convective turbulence may transport low-level aerosol upward to high altitude, and the high temperature and relative humidity favors the production of aerosol precursors and the growth of existing particles (Xia et al., 2006; Che et al., 2009), which will increase aerosol backward scattering, and thus lead to high AOD values. In winter, the northern cold, dry and clean winter monsoon affects China, and the cold air activities with large wind speed contribute to the aerosol dispersion in this season. Therefore, AOD values are low in winter. February appears as an outlier for both sites probably because of extensive fireworks during the spring holidays (from 2 to 8 February 2011). However, Fig. 4a shows that in some months, the AOD values measured in the urban site are higher, while in some other months the AOD values measured at the urban site are lower. This indicates that the AODs measured at the urban and rural sites do not explain the difference in the shortwave radiation observed in Fig. 3. To investigate the difference between the two sites in AOD at longer time scales, the monthly-averaged AOD values at four wavelengths between 2010 and 2012 are compared (Fig. 4b). A linear fitting suggests that the AOD values at the Xianghe (rural) site are 0.96 (with a standard error of 0.02) times the AOD values at the Beijing (urban) site, implying that the AOD values at the urban site are slightly larger than those at the rural site at longer time scales. This is in agreement with the factual heavier air pollution as a result of urbanization.

The AOD measurements used herein are all cloud-screened; that is, all AOD values are retrieved under clear-sky conditions. However, the presence of clouds can also significantly modify the surface energy balance, particularly by altering the incoming shortwave radiation. There have been many studies devoted to analyzing the impact of urbanization on cloud processes and precipitation [see Shephard (2005) for a review]. The principal mechanisms are urban heat island effects (e.g., Bornstein and Lin, 2000; Lin et al., 2011; Miao et al., 2011), urban canopy effects (e.g., Loose and Bornstein, 1977; Miao et al., 2011), and urban aerosol effects (e.g., Jin and Shepherd, 2008; Ntelekos et al., 2009; Jin et al., 2010).

All of these mechanisms can have an impact on cloud formation. For instance, as a result of the urban heat island effect, thermal convection in urban environments will be enhanced and more clouds are likely to form over cities. In our study, the cloud conditions at the urban and rural sites are examined using satellite observations. The cloud fraction product from MODIS is used. Figure 5a shows the monthly-averaged cloud fractions at the two sites in 2011. It is clear that the two sites generally have more clouds in summer than in winter, with February as an outlier. The seasonal variability of cloud fractions clearly resembles that of AOD at the two sites, implying significant aerosol–cloud interactions. Yuan et al. (2011) also found that cloud fraction changes with aerosol loading. Concerning the differences between the two sites, the urban cloud fractions are larger than their rural counterparts, except in April, May, June and November. For these months, the AOD values at the urban site are larger than their rural counterparts in May and November (see Fig. 4a). As a result, the combination of aerosol and cloud information seems to explain a large part of the difference between the two sites in incoming shortwave radiation. It is, however, noted that the cloud fraction estimates have relatively large uncertainties given that measurements are only available a few times (usually two to four) a day. Similar to Fig. 4b, to further quantify the difference in cloud fractions between the two sites, we use monthly-averaged data from 2010 to 2012, as shown in Fig. 5b. Linear fitting is also conducted: $y = 1.00x$ (the slope 1.00 has a standard error of 0.01), where x and y are the cloud fractions at the Beijing and Xianghe sites, respectively. As such, the difference in cloud fractions at these two sites is not significant over these three years.

The incoming longwave radiation received at the surface is predominantly emitted by clouds, water vapor (quantified in terms of precipitable water), and other greenhouse gases such as carbon dioxide and ozone in the atmosphere. It varies with both the amount and properties of these constituents. The vertical distribution of air temperature also has a significant impact on the incoming longwave radiation: the incoming longwave radiation generally increases with the air temperature. The monthly-averaged precipitable water in 2011 measured at the two sites by AERONET is shown in Fig. 6a. In general, the Xianghe site has relatively higher precipitable water than the Beijing site. This is further confirmed by comparing the precipitable water at the two sites for the period from 2010 to 2012 (Fig. 6b). As can be seen from Fig. 6b, the linear fitting indicates that the precipitable water at the Xianghe site is slightly larger than at the Beijing site (slope is 1.05 with a standard error of 0.01), especially when the amount of precipitable water is large. The lower precipitable water at the urban site is probably due to reduced evapotranspiration in urban areas. Nonetheless, precipitable water alone cannot explain the observed longwave radiation differences between the two sites, since Fig. 6b would suggest that the urban site has less longwave radiation than the rural site, contrary to the actual observation shown in Fig. 3. Given that water vapor is the most abundant greenhouse gas in the atmosphere, it is concluded that the observed differences in the longwave radiation cannot be explained solely by the presence of more greenhouse gases over cities as suggested by Oke (1982). The larger longwave radiation at the urban site (Fig. 3) is most likely caused by the higher air temperature, i.e., the urban heat island effect.

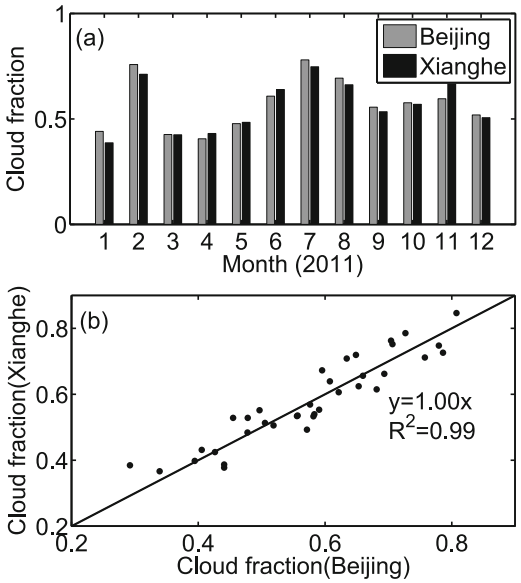

Fig. 5. (a) Monthly-averaged cloud fraction at Beijing and Xianghe in 2011, and (b) comparison of monthly-averaged cloud fraction at Beijing and Xianghe from 2010 to 2012.

3.2. *Turbulent exchanges at the urban and rural sites*

In this section, the turbulent exchanges of sensible heat and latent heat are examined at the two sites. They are important components in the surface energy balance equation [Eq. (1)] and their measurements are available at both sites.

Figure 7 shows the monthly-averaged diurnal cycles of the net radiation [calculated from Eq. (2)], sensible heat flux (H), latent heat flux (LE), and the heat storage (calculated as $R_n - H - \mathrm{LE}$, by temporarily omitting the anthropogenic heat flux Q_F here, because of the absence of accurate energy consumption and traffic flow data) at the Beijing site in 2011. As mentioned in section 2, the measurements are available at three levels: 47 m, 140 m and 280 m. As can be seen from Fig. 7, the net radiation is larger in spring and summer than in autumn and winter. The seasonal variations of net radiation generally follow those of incoming shortwave radiation (Fig. 3). The sensible heat fluxes peak (~ 200 W m^{-2}) in March, April and May, mostly because of the larger net radiation during this period. In other months, the monthly-averaged diurnal cycles of sensible heat flux are fairly similar, with peak values of about 100 W m^{-2}. In contrast, there is a strong seasonality in the latent heat flux, which reaches its maximum values (~ 150 W m^{-2}) in the summer months (June, July and August) and diminishes significantly in the winter months (November, December, January and February). The heat storage is the largest amongst the surface energy budget terms, whose peak value reaches 350 W m^{-2} in the spring

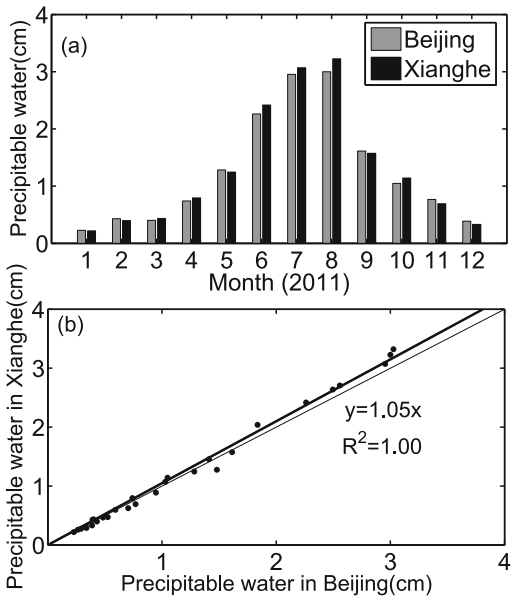

Fig. 6. (a) Monthly-averaged precipitable water (cm) at the Beijing and Xianghe sites in 2011 and (b) comparison of monthly-averaged precipitable water (cm) at the Beijing and Xianghe sites from 2010 to 2012.

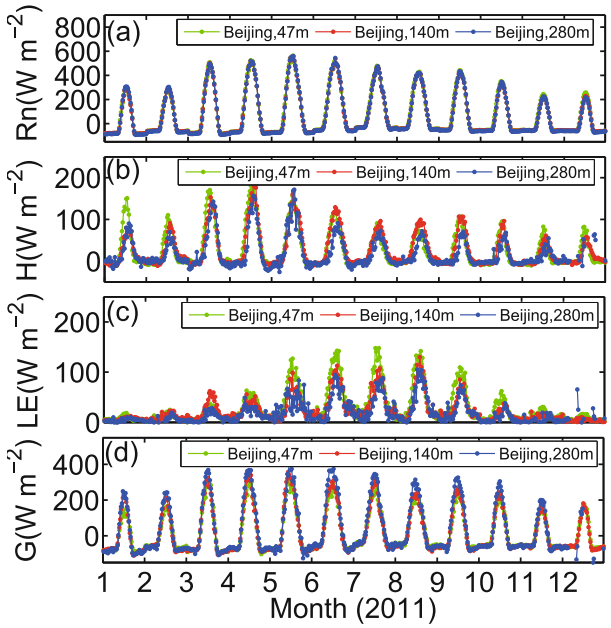

Fig. 7. Monthly-averaged diurnal cycles of (a) net radiation, (b) sensible heat flux, (c) latent heat fluxes, and (d) heat storage at the Beijing site in 2011.

and summer months. This implies that a significant portion of the driving energy flux is stored in the urban canopy and ground, causing the urban heat island effect. The variations in the heat storage also follow those of the net radiation, and thus those of the incoming solar radiation. The fluxes measured at the three levels are inter-compared (not shown here). The net radiation measured at the three different levels are very close to each other and the differences are within 1% to 2%. The sensible heat fluxes measured at 47 m and 140 m are fairly close to each other, while those measured at 280 m are significantly lower. Larger differences (10%–30%) are observed for latent heat fluxes and heat storages: the latent heat fluxes decrease with the height and the heat storage increases with the height. It is interesting to note that these results are not directly inferable from the land-use and land-cover information provided in Table 1. According to this information, the footprint corresponding to the measurements at 280 m has the highest cropland fraction, yet our observations indicate the level corresponds to the smallest latent heat flux. A more accurate model for estimating footprints in such a heterogeneous environment and a detailed analysis of the composition of footprints are needed to completely understand the vertical variations of turbulent fluxes. In the following analysis when we compare the urban fluxes to rural fluxes, only the fluxes measured at 140 m are used. This is because the other two levels are not in the constant-flux layer (Miao et al., 2012).

Due to data availability, only sensible heat and latent heat fluxes at the Xianghe site are analyzed and compared to those measured at the Beijing site. As can be seen from Fig. 8, seasonal variations in the sensible heat flux at the Xianghe site are similar to those observed at the Beijing site, while the peak values are lower for the former. The latent heat fluxes at the Xianghe site also reach their maximum in the growing season, i.e. May, June, July and August, because of the monsoon wet season. This is also similar to what is observed at the Beijing site. When fluxes at the two levels are compared at the Xianghe site, the differences are relatively small compared to those observed at the Beijing site. The sensible heat flux at 32 m is about 10% larger than that at 64 m, while the latent heat fluxes at the two levels are very close. This implies that the two levels are both in the constant-flux layer. As such, we choose the arithmetic mean of fluxes at the two

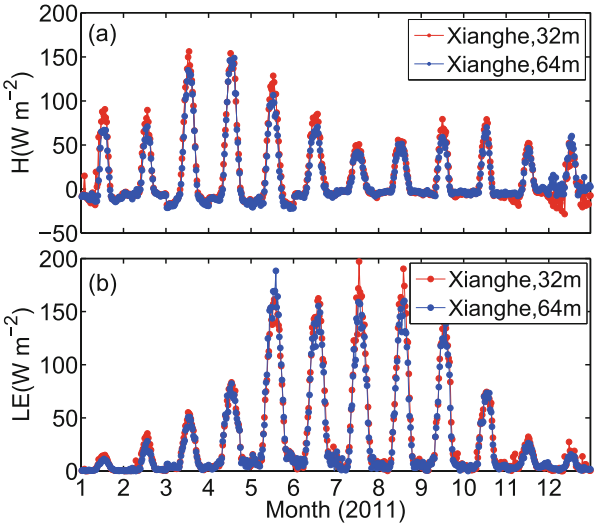

Fig. 8. Monthly-averaged diurnal cycles of (a) sensible heat and (b) latent heat fluxes at the Xianghe site in 2011.

levels as a reference for urban–rural comparisons.

Figure 9 shows the differences between the urban and rural sensible heat flux, latent heat flux, and available energy. The available energy is the sum of the sensible and latent heat fluxes. It is clear that the urban site has higher sensible heat fluxes and, overall, lower latent heat fluxes. The differences in the sensible heat fluxes are most evident from April to September, and the maximum in the differences does not concur with the maximum in the sensible heat fluxes. For the latent heat fluxes, the largest difference occurs in May. The differences are then reduced in June and maintained at relatively low values throughout the growing season until October. The intra-annual variations in the urban–rural contrast in evapotranspiration suggest that the difference in evapotranspiration is not only related to the difference in green cover fraction, but also the difference in soil moisture availability. An examination reveals that the increase in latent heat fluxes just before the growing season (in May) is much more significant at the Xianghe site, which is attributed to three factors: (1) the Xianghe site has a larger fraction of cropland, leading to a more rapid increase in evapotranspiration; (2) the soil moisture at the Xianghe site is not a limiting factor for crop growth; and (3) the growing vegetation contributes a larger amount of water vapor to the atmosphere. The difference between the urban and rural available energy is also very important, e.g. in estimating the strength of the urban heat island effect (Li and Bou-Zeid, 2013). It is interesting to observe that the urban available energy is generally larger than its rural counterpart, which, according to Li and Bou-Zeid (2013) will cause the urban heat island effect. The only two outliers occur just before and just after the growing season, i.e. May and October. The outlier in May is because of the faster increase in evapotranspiration at the beginning of the growing season at the rural site, which was mentioned before. The outlier in October is due to the sharper decrease in evapotranspiration at the end of the growing season at the urban site, which is probably due to the soil moisture limitation in urban areas. Both are related to the contrast in surface water availability between the urban and rural sites.

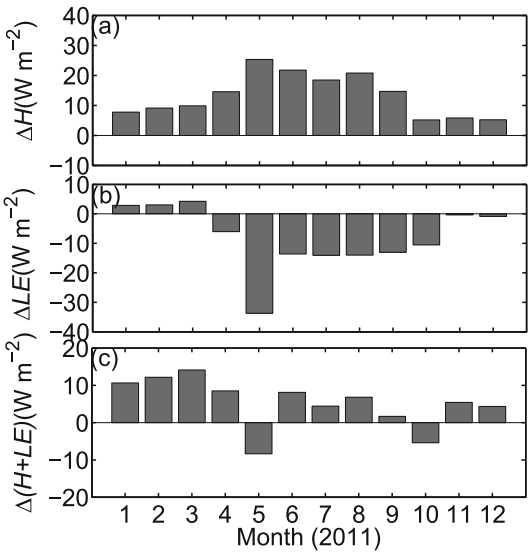

Fig. 9. Monthly-averaged differences in (a) sensible heat flux ΔH, (b) latent heat flux ΔLE, and (c) available energy $\Delta(H + \mathrm{LE})$ between the Beijing and Xianghe sites in 2011.

4. Discussion and conclusions

A direct comparison of urban and rural surface energy balances, as well as a variety of other meteorological variables, is conducted for the Beijing metropolitan area. The main conclusions reached in this study are as follows:

The framework proposed by Oke (1982) remains the paradigm for understanding urban–rural contrasts in the surface energy balance, but should be subjected to some modifications. The field experiments conducted over the densely populated Beijing metropolitan area suggest that compared to rural areas, the urban areas generally receive less shortwave radiation but more longwave radiation. Nonetheless, the observed differences are not merely associated with urban pollution as suggested by Oke (1982). We found that neither AOD nor cloud fraction alone can explain the difference in the incoming shortwave radiation. It is possible that a combination of aerosol and cloud information can explain a large part of the difference, but this needs to be verified using more sophisticated radiation models. In addition, we try to attribute the differences in the incoming longwave radiation to the amount of greenhouse gases, as also suggested by Oke (1982). Given that water vapor is the most abundant greenhouse gas, the precipitable water is compared and it is found that the urban areas have less precipitable water. As such, the larger longwave radiation received in the urban areas is unlikely to be caused by the differences in the amount of greenhouse gases.

The urban surface–atmosphere exchanges of sensible heat and latent heat differ from their counterparts in rural areas. In general, urban areas produce higher sensible heat fluxes and lower latent heat fluxes. The urban–rural contrasts in the surface energy balance also show seasonal variations. The maximum differences in both sensible heat and latent heat fluxes are found to occur in boreal summer. Urban areas also produce a larger amount of available energy than the rural areas, which is an important contributor to the urban heat island effect. This is not the case just before and just after the growing season, due to the faster increase in evapotranspiration in rural areas just before the growing season and the sharper decrease in evapotranspiration in urban areas just after the growing season. Both are related to the surface moisture limitation in urban areas compared to rural areas.

The above findings have important implications for urban modeling and urban management. First, it calls for a more accurate representation of aerosol–cloud interactions in numerical weather and climate models. Second, even for such densely populated urban terrain, evapotranspiration remains a significant component in the surface energy balance. The urban modules used in numerical weather and climate models

need to take into account urban hydrological processes, hence the method of parameterizing an urban area as a completely impervious surface is inappropriate. Third, the difference in evapotranspiration between urban and rural areas is not only related to the difference in green cover (i.e., grass and trees) fraction, but also the difference in soil moisture conditions. Urban irrigation can be helpful in promoting evapotranspiration and thus alleviating the urban heat stresses.

Acknowledgements. This study was supported by the National Key Basic Research Program (Grant Nos. 2010CB428502 and 2012CB417203), the National Natural Science Foundation of China (Grant Nos. 41405018 and 41275022), the China Meteorological Administration (Grant No. GYHY201006024), and the CAS Strategic Priority Research Program (Grant No. XDA05110101). We acknowledge CHEN Hongbin (Chinese Academy of Sciences) and P. GOLOUB (Université Lille 1) as co-PIs and Service d'Observation PHOTONS/AERONET from INSU/CNRS for maintaining and calibrating the AERONET instruments. Our special thanks go to Prof. XIA Xiangao for providing the radiation flux data for the Xianghe site. GUO Xiaofeng acknowledges the support of the State Key Laboratory of Atmospheric Boundary Layer Physics and Atmospheric Chemistry, Institute of Atmospheric Physics, Chinese Academy of Sciences (Grant No. LAPC-KF-2009-02).

REFERENCES

Arnfield, A. J., 2003: Two decades of urban climate research: A review of turbulence, exchanges of energy and water, and the urban heat island. *Int. J. Climatol.*, **23**(1), 1–26.

Bornstein, R., and Q. L. Lin, 2000: Urban heat islands and summertime convective thunderstorms in Atlanta: Three case studies. *Atmos. Environ.*, **34**(3), 507–516.

Britter, R. E., and S. R. Hanna, 2003: Flow and dispersion in urban areas. *Annu. Rev. Fluid. Mech.*, **35**, 469–496.

Brutsaert, W., 1982: *Evaporation into the Atmosphere: Theory, History, and Applications*. Springer, Netherlands, 299 pp.

Che, H. Z., and Coauthors, 2009: Instrument calibration and aerosol optical depth validation of the China Aerosol Remote Sensing Network. *J. Geophys. Res.*, **114**, D03206, doi: 10.1029/2008JD011030.

Chen, F., and Coauthors, 2011: The integrated WRF/urban modelling system: Development, evaluation, and applications to urban environmental problems. *Int. J. Climatol.*, **31**(2), 273–288.

Cleugh, H. A., and T. R. Oke, 1986: Suburban-rural energy-balance comparisons in summer for Vancouver, B. C. *Bound.-Layer Meteor.*, **36**(4), 351–369.

Eck, T. F., B. N. Holben, J. S. Reid, O. Dubovik, A. Smirnov, N. T. O'Neill, I. Slutsker, and S. Kinne, 1999: Wavelength dependence of the optical depth of biomass burning, urban, and desert dust aerosols. *J. Geophys. Res.*, **104**(D24), 31 333–31 349.

Gong, P., and Coauthors, 2012: Finer resolution observation and monitoring of global land cover: First mapping results with Landsat TM and ETM+ data. *Int. J. Remote Sens.*, **34**(7), 2607–2654.

Grimm, N. B., S. H. Faeth, N. E. Golubiewski, C. L. Redman, J. G. Wu, X. M. Bai, and J. M. Briggs, 2008: Global change and the ecology of cities. *Science*, **319**(5864), 756–760.

Grimmond, C. S. B., and T. R. Oke, 1995: Comparison of heat fluxes from summertime observations in the suburbs of 4 North-American cities. *J. Appl. Meteor.*, **34**(4), 873–889.

Grimmond, C. S. B., and T. R. Oke, 1999: Heat storage in urban areas: Local-scale observations and evaluation of a simple model. *J. Appl. Meteor.*, **38**(7), 922–940.

Grimmond, C. S. B., T. R. Oke, and H. A. Cleugh, 1993: The role of "rural" in comparisons of observed suburban-rural flux differences. Exchange processes at the land surface for a range of space and time scales, *International Association of Hydrological Sciences Publication*, **212**, 165–174.

Grimmond, C. S. B., and Coauthors, 2010: The international urban energy balance models comparison project: First results from phase 1. *J. Appl. Meteor. Climol.*, **49**(6), 1268–1292.

Grimmond, C. S. B., and Coauthors, 2011: Initial results from Phase 2 of the international urban energy balance model comparison. *Int. J. Climatol.*, **31**(2), 244–272.

Grimmond, S., 2007: Urbanization and global environmental change: Local effects of urban warming. *Geophys. J.*, **173**, 83–88.

Hu, X. M., P. M. Klein, M. Xue, J. K. Lundquist, F. Zhang, and Y. Qi, 2013: Impact of low-level jets on the nocturnal urban heat island intensity in Oklahoma City. *J. Appl. Meteor. Climatol.*, **52**(8), 1779–1802.

Holben, B. N., and Coauthors, 1998: AERONET-A federated instrument network and data archive for aerosol characterization. *Remote. Sens. Environ.*, **66**(1), 1–16.

Jin, M. L., and J. M. Shepherd, 2008: Aerosol relationships to warm season clouds and rainfall at monthly scales over east China: Urban land versus ocean. *J. Geophys. Res.*, **113**, doi: 10.1029/2008JD010276.

Jin, M. L., J. M. Shepherd, and W. Z. Zheng, 2010: Urban surface temperature reduction via the urban aerosol direct effect: A remote sensing and WRF model sensitivity study. *Adv. Meteor.*, Article ID 681587, doi: 10.1155/2010/681587.

Kanda, M., 2007: Progress in urban meteorology: A review. *J. Meteor. Soc. Japan*, **85B**, 363–383.

Kanda, M., R. Moriwak, M. Roth, and T. Oke, 2002: Area-averaged sensible heat flux and a new method to determine zero-plane displacement length over an urban surface using scintillometry. *Bound.-Layer Meteor.*, **105**(1), 177–193.

Li, D., and E. Bou-Zeid, 2011: Coherent structures and the dissimilarity of turbulent transport of momentum and scalars in the unstable atmospheric surface layer. *Bound.-Layer Meteor.*, **140**(2), 243–262.

Li, D., and E. Bou-Zeid, 2013: Synergistic interactions between urban heat islands and heat waves: The impact in cities is larger than the sum of its parts. *J. Appl. Meteor. Climtol.*, **52**, 2051–2064.

Li, D., E. Bou-Zeid, M. L. Baeck, S. Jessup, and J. A. Smith, 2013: Modeling land surface processes and heavy rainfall in urban environments: Sensitivity to urban surface representations. *J. Hydrometeor.*, **14**, 1098–1118.

Li, Q. S., L. H. Zhi, and F. Hu, 2010: Boundary layer wind structure from observations on a 325 m tower. *J. Wind Eng. Ind. Aerodyn.*, **98**(12), 818–832.

Lin, C. Y., W. C. Chen, P. L. Chang, and Y. F. Sheng, 2011: Impact of the urban heat island effect on precipitation over a complex geographic environment in Northern Taiwan. *J. Appl. Meteor. Climtol.*, **50**(2), 339–353.

Loose, T., and R. D. Bornstein, 1977: Observations of mesoscale

effects on frontal movement through an urban area. *Mon. Wea. Rev.*, **105**(5), 563–571.

Loridan, T., and C. S. B. Grimmond, 2012: Characterization of energy flux partitioning in urban environments: Links with surface seasonal properties. *J. Appl. Meteor. Climatol.*, **51**(2), 219–241.

Miao, S. G., P. Y. Li., and X. Y. Wang, 2009: Building morphological characteristics and their effect on the wind in Beijing. *Adv. Atmos. Sci*., **26**(6), 1115–1124, doi: 10.1007/s00376-009-7223-7.

Miao, S. G., F. Chen, Q. C. Li, and S. Y. Fan, 2011: Impacts of urban processes and urbanization on summer precipitation: A case study of heavy rainfall in Beijing on 1 August 2006. *J. Appl. Meteor. Climatol.*, **50**(4), 806–825.

Miao, S. G., J. X. Dou, F. Chen, J. Li, and A. G. Li, 2012: Analysis of observations on the urban surface energy balance in Beijing. *Sci. China Earth Sci.*, **55**(11), 1881–1890.

Nordbo, A., L. Järvi, S. Haapanala, J. Moilanen, and T. Vesala, 2013: Intra-city variation in urban morphology and turbulence structure in Helsinki, Finland. *Bound.-Layer Meteor.*, **146**(3), 469–496.

Ntelekos, A. A., J. A. Smith, L. Donner, J. D. Fast, W. I. Gustafson, E. G. Chapman, and W. F. Krajewski, 2009: The effects of aerosols on intense convective precipitation in the northeastern United States. *Quart. J. Roy. Meteor. Soc.*, **135**(643), 1367–1391.

O'Neill, N. T., T. F. Eck, A. Smirnov, B. N. Holben, and S. Thulasiraman, 2003: Spectral discrimination of coarse and fine mode optical depth. *J. Geophys. Res.*, **108**, 4559, doi: 10.1029/2002JD002975.

Oke, T. R., 1982: The energetic basis of the urban heat island. *Quart. J. Roy. Meteor. Soc.*, **108**(455), 1–24.

Peterson, J. T., and T. L. Stoffel, 1980: Analysis of urban-rural solar-radiation data from St-Louis, Missouri. *J. Appl. Meteor.*, **19**(3), 275–283.

Piringer, M., and Coauthors, 2002: Investigating the surface energy balance in urban areas-recent advances and future needs. *Water, Air, and Soil Pollution: Focus*, **2**(5–6), 1–16.

Rosenfeld, D., U. Lohmann, G. B. Raga, C. D. O'Dowd, M. Kulmala, S. Fuzzi, A. Reissell, and M. O. Andreae, 2008: Flood or drought: How do aerosols affect precipitation? *Science*, **321**(5894), 1309–1313.

Shephard, J. M., 2005: A review of current investigations of urban-induced rainfall and recommmendations for the future. *Earth Interact*, **9**, 1–27.

Tan, M. H., and X. B. Li, 2013: Integrated assessment of the cool island intensity of green spaces in the mega city of Beijing. *Int. J. Remote Sens*., **34**(8), 3028–3043.

The Office of the Sixth National Census Beijing (OSCB), 2011: The characteristics of Beijing's population distribution. [Available online at http://www.bjstats.gov.cn/rkpc_6/pcsj/ (Accessed Mar 19, 2013).]

Wang, L. L., D. Li, Z. Q. Gao, T. Sun, X. F. Guo, and E. Bou-Zeid, 2014: Turbulent transport of momentum and scalars above an urban canopy. *Bound.-Layer Meteor.*, **150**, 485–511.

Wood, C. R., and Coauthors, 2010: Turbulent flow at 190 m height above London during 2006–2008: A climatology and the applicability of similarity theory. *Bound.-Layer Meteor.*, **137**(1), 77–96.

Xia, X. A., H. B. Chen, P. C. Wang, W. X. Zhang, P. Goloub, B. Chatenet, T. F. Eck, and B. N. Holben, 2006: Variation of column-integrated aerosol properties in a Chinese urban region. *J. Geophys. Res.*, **111**(D5), doi: 10.1029/2005JD006203.

Xia, X. A., Z. Li, P. Wang, H. Chen, and M. Cribb, 2007: Estimation of aerosol effects on surface irradiance based on measurements and radiative transfer model simulations in northern China. *J. Geophys. Res.*, **112**(D22), doi: 10.1029/2006JD008337.

Yuan, T., L. A. Remer, and H. Yu, 2011: Macrophysical, microphysical and radiative signatures of volcanic aerosols in trade wind cumulus observed by the A-Train. *Atmos. Chem. Phys*., **11**, 7119–7132, doi: 10.5194/acp-11-6415-2011.

Zhang, C. L., F. Chen, S. G. Miao, Q. C. Li, X. A. Xia, and C. Y. Xuan, 2009: Impacts of urban expansion and future green planting on summer precipitation in the Beijing metropolitan area. *J. Geophys. Res.*, **114**, D02116, doi: 10.1029/2008JD010328.

Zhang, N., L. Zhu, and Y. Zhu, 2011: Urban heat island and boundary layer structures under hot weather synoptic conditions: A case study of Suzhou City, China. *Adv. Atmos. Sci*., **28**(4), 855–865, doi: 10.1007/s00376-010-0040-1.